Int. J. Heat Mass Transfer. Vol. 35, No. 11, pp. 3115–3129, 1992
Printed in Great Britain

0017-9310/92 $5.00+0.00

Numerical and experimental studies of self-sustained oscillatory flows in communicating channels

C. H. AMON and D. MAJUMDAR
Carnegie Mellon University, Pittsburgh, PA 15213, U.S.A.

C. V. HERMAN and F. MAYINGER
Technical University of Munich, 8000 Munich, Germany

B. B. MIKIC
Massachusetts Institute of Technology, Cambridge, MA 02139, U.S.A.

and

D. P. SEKULIC
University of Novi Sad, 21000 Novi Sad, Yugoslavia

(*Received* 10 *April* 1991 *and in final form* 21 *October* 1991)

Abstract—A combined numerical and experimental investigation of flow fields and thermal phenomena in communicating channels is performed to gain insight into the operation of compact heat exchange surfaces with interrupted plates. The geometric parameters are selected to excite and sustain the normally damped Tollmien–Schlichting modes. As a result, traveling waves are observed at relatively low Reynolds numbers, inducing self-sustained oscillatory flows that significantly enhance mixing. The critical Reynolds number at which oscillations are first observed in the periodic, fully developed flow region is determined. The numerical results are obtained by *direct* numerical simulation of the time-dependent energy and Navier–Stokes equations using a spectral element–Fourier method. The oscillatory heat transfer phenomenon is visualized experimentally using real-time, holographic interferometry. For periodic, fully developed flow conditions, the temperature fields are recorded utilizing high-speed cinematography. The experimental visualizations of the thermal waves verify the numerical predictions of the thermal-fluid structure and evolution of communicating-channels flows.

1. INTRODUCTION

THE DEVELOPMENT of compact heat transfer surfaces has received much attention in the engineering community motivated by the necessity to reduce the size and weight of heat exchange devices such as those encountered in automobiles, air conditioning, electronic cooling, spacecraft and aircraft. These devices usually operate at moderate Reynolds numbers.

A commonly used technique for improving the performance of heat exchange devices is to employ heat transfer surfaces that are periodically interrupted along the streamwise direction (i.e. rectangular plate-fin, offset-fin, offset strip-fin and louvered-fin) [1, 2]. Such an arrangement may be viewed as a succession of flat-plate segments aligned parallel to the flow with gaps between successive plates. A typical geometry, referred to as communicating-channels geometry, is shown schematically in Fig. 1. Previous research work on the overall heat transfer and pressure drop performance in similar geometries is presented in refs. [3, 4]. High-heat transfer effectiveness is obtained in these surfaces as a result of the relatively thin boundary layers induced by their periodic formation at the interrupted surfaces. It has been shown that additional improvement in the heat transfer performance is achieved when the flow undergoes transition to unsteady, self-sustained oscillatory flow [5, 6]. Numerical simulations of these oscillatory flows indicate that heat transfer enhancement is due to the interruption of boundary layers as well as the communication between channels and mixing produced by self-sustained oscillations [7].

The understanding of the convection mechanisms and the prediction of heat transfer performance in compact heat exchangers has motivated different investigative procedures including data acquisition for actual and scaled-up models, empirical correlations, analytical models, flow visualizations, mass transfer experiments and numerical simulations [8]. Basically, three broad approaches have been followed, namely, acquisition and correlation of empirical data, qualitative observations of the convection processes and numerical solutions with analytical modeling. The first approach has yielded a large amount of empirical information [1]. In the work described here, we com-

NOMENCLATURE

a	half-separation distance between channels (Fig. 1) [m]
D	computational domain
f	pressure gradient
h	heat transfer coefficient
H	half-channel height [m]
k	thermal conductivity [W m^{-1} K^{-1}]
l	separation distance between plates (Fig. 1) [m]
L	periodicity length (Fig. 1) [m]
L^*	wavelength [m]
n	periodicity index
Nu	Nusselt number, hH/k
P	pressure
Pr	Prandtl number, ν/α
q''	heat flux per unit area
Q	flow rate
R	Reynolds number, $(3/2)VH/\nu$
t	non-dimensional time
t^*	time [s]
T	temperature
T_p	heated plate temperature [°C]
u, v	velocity components in the x- and y-directions, respectively
v	velocity vector
V	channel-averaged velocity
w	channel width [m].

Greek symbols

α	thermal diffusivity [m^2 s^{-1}]
β	streamwise wavenumber
Δp	pressure drop between entry and exit of test section [N m^{-2}]
∂D_s	solid wall boundary of D
∂D_p	periodic boundary
θ	periodic temperature
λ	wavelength of laser light [m]
ν	kinematic viscosity [m^2 s^{-1}]
Π	dynamic pressure
ω	angular frequency
ω	vorticity.

Subscripts

c	critical
d	dimensional
in	channel inlet
out	channel outlet
o	refers to basic geometry (plane channel)
p	periodic
s	solid wall
TS	Tollmien–Schlichting.

bine the last two approaches and perform detailed numerical simulations complemented by experimental observations in order to achieve a better understanding of the complex fluid flow and transport phenomena in compact heat transfer surfaces.

This study is concerned with heat exchanger regions sufficiently far downstream where entrance effects are negligible and, therefore, periodic, fully developed flow field and heat transfer conditions are obtained. The periodic, fully developed concepts, introduced by Patankar *et al.* [9] for steady-state conditions, are extended here to solve time-dependent problems.

2. METHOD OF STUDY

The internal flow pattern and heat transfer characteristics are investigated both experimentally and numerically in the periodic, fully developed region of the two-dimensional, communicating-channels geometry shown in Fig. 1. This geometry consists of a succession of colinear plate segments aligned parallel to the flow. The flow configuration for the experimental setup and numerical calculations can be geometrically described by the following non-dimensional parameters: geometric periodicity length

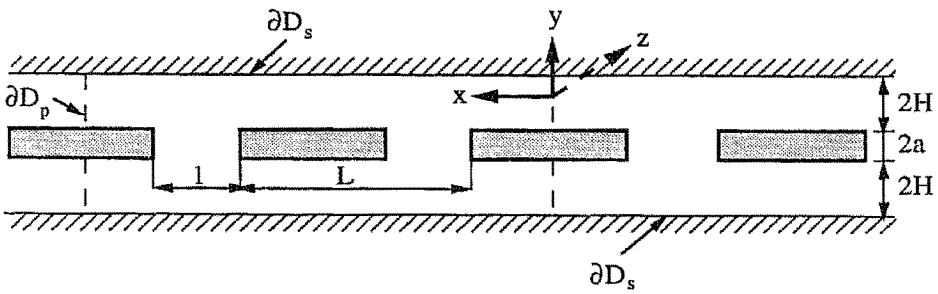

FIG. 1. Geometry of the periodic communicating channels described by the plates spacing l, the separation distance between channels $2a$ and the periodicity length L. The dimensions of the experimental test section are: $l = 0.015$ m, $2a = 0.005$ m, $L = 0.04$ m and $2H = 0.01$ m.

$L/H = 8$, plate spacing $l/H = 3$, and separation between channels $2a/H = 1$. The working fluid is air, and the direction of the air flow is from right to left. The top and bottom flat walls are adiabatic, and the thermal boundary condition on the heated plates is characterized by constant heat flux.

The experimental test section contains ten heated plates. At a sufficient downstream distance, a periodic, fully developed flow regime is established where the instantaneous velocity and scaled temperature profiles repeat periodically in space. The experimental measurements described in this paper were performed on the ninth and tenth plates. The isotherms were visualized using the infinite fringe field arrangement of holographic interferometry and were recorded by high-speed cinematography with velocities of up to 600 frames per second. Non-stationary phenomena were thus registered, providing insight into the complex physical process of heat transfer in communicating channels.

The numerical results presented here were obtained by direct numerical simulation of the two-dimensional Navier–Stokes and energy equations, starting with arbitrary initial conditions and advancing in time until a steady or time-periodic state was found.

3. EXPERIMENTAL EQUIPMENT AND PROCEDURE

The experimental duct has a rectangular cross section with parallel walls, a total height $(4H+2a)/H = 5$ and width $w/H = 30$. The interrupted plates are represented by a succession of parallel plate segments positioned in the central plane of the duct, constituting the two communicating channels, each one of height $2H$ (Fig. 1). The experimental setup used in the visualization of the temperature fields in the communicating channels is presented in Fig. 2. The parallel plate duct is horizontally positioned and consists of entry, test and exit sections of length $60H$, $100H$ and $60H$, respectively. Ten heated copper plates are positioned in the central plane of the test section and held by Plexiglas holders. The viewing window, whose size matches the diameter of the expanded laser beam, is manufactured of glass to avoid influence of the window material on the interferometric image. The temperature of the top wall of the test section is monitored by 17 nickel–chrome–constantan thermocouples to provide reference temperature values. The exit section is equipped with a blower that operates in the suction mode, force-convecting the air flow. Four pressure taps of 0.0001 m in diameter are located in each of the flanges between the entry section and the test section and between the test section and the exit section. A pressure transducer (Setra Series 239) calibrated by a Betz manometer is used for pressure drop measurements.

The structure and dimensions of the heated copper plates are presented schematically in Fig. 3. Each plate consists of two halves enclosing the electric foil heater. In the top and bottom surfaces, two constantan–manganin 0.0001 m diameter thermocouples were inserted and positioned as indicated in Fig. 3. The thermocouples allow for accurate measurements of plate temperatures providing reference values for the interpretation of interferometric images. The desired temperature of the heated plates is achieved by varying the DC supply voltage to the foil heater. The temperature increase along the test section ($T_{out} - T_{in}$, Fig. 2) is measured by two batteries of nickel–chrome–constantan thermocouples. Each battery consists of five thermocouples connected in series and distributed over the cross-sectional area, providing average temperature values and yielding amplified emf for enhanced accuracy. Air flow velocity profile measurements at the end of the entry section are obtained by a Schiltknecht hot wire anemometer thermo-air type 442 which was previously calibrated by a rotameter.

To visualize the time-dependent temperature fields in the communicating channels, a field measurement

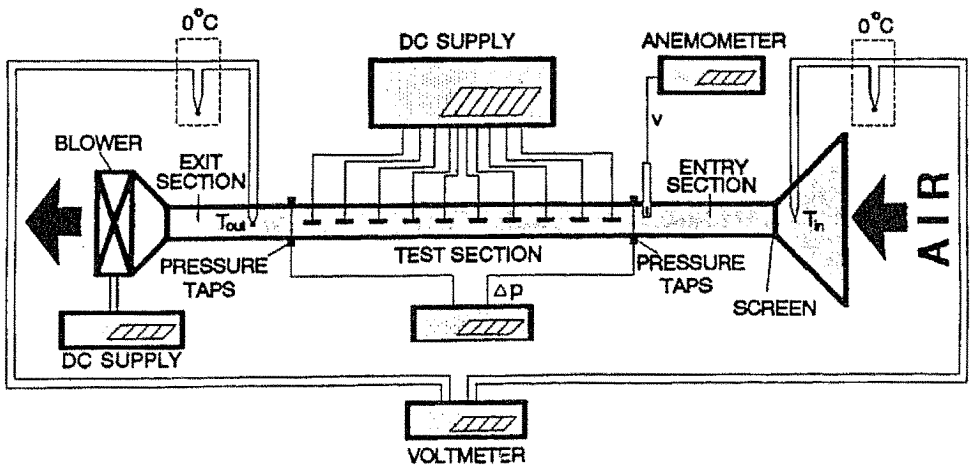

FIG. 2. Schematic of the experimental setup.

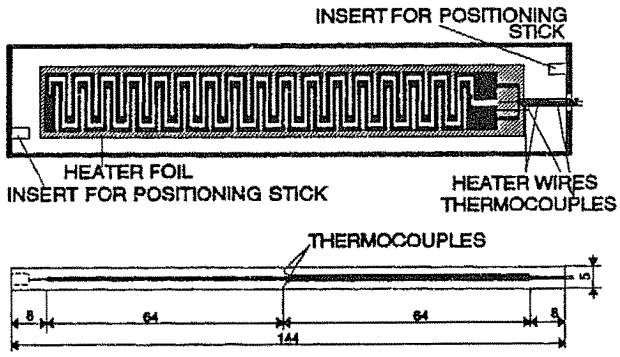

FIG. 3. Schematic of the heated copper plates.

technique was implemented which provides two-dimensional data in each measurement [10]. The real-time method of holographic interferometry was selected since it enables visualization and quantitative measurement of temperatures with high spatial and temporal resolutions without disturbing the investigated physical phenomena. The resolution is only limited by the sensitivity of the photographic material and by the mechanical limitations of the film speed. The principles and applications of holography and interferometry in heat transfer measurements have been treated in detail in the literature [11–14].

Figure 4 shows the optical setup used for holographic interferometry visualizations, and more details on the experimental arrangement are given in [10]. A He–Ne laser with 0.632 m wavelength, 0.03 W power and 0.2 m coherence length served as the light source. In the experiments, real-time methods with high-speed recordings of the interferograms were used. The reference state of the process, corresponding to the experimental setup at ambient temperature, was first recorded on the holographic plate. The holographic plate was then processed and afterwards accurately repositioned into its original location using a precision plate holder. Then the investigated phenomenon was examined. The high-speed recordings of the interferograms were taken at film velocities from 150 to 600 frames per second with recording intervals of approximately 5 s. The high-speed film enables the evaluation of high-frequency oscillatory temperature fields, whereas the interferograms, observed with a naked eye, give only an indication of the non-stationary nature of this phenomenon, since the image appears as a mild, unsteady vibration.

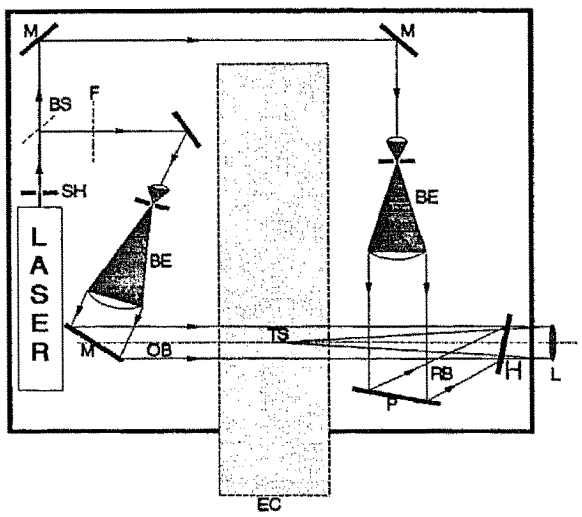

FIG. 4. Optical arrangement for holographic interferometry.

4. MATHEMATICAL FORMULATION AND NUMERICAL SOLUTION TECHNIQUE

The numerical part of this work deals with finding periodic, fully developed characteristics of the flow field and heat transfer. The computational domain can, therefore, be restricted to a region comprising an integer number, n, of geometric periodicity such as the region between the dotted lines shown in Fig. 1. This enables us to impose periodic flow conditions and obtain fully developed solutions without considering the entrance region.

We consider Newtonian, incompressible, two-dimensional flows with constant properties, which are governed by the unsteady Navier–Stokes and energy equations written in the following non-dimensional form

$$\frac{\partial \mathbf{v}}{\partial t} = \mathbf{v} \times \boldsymbol{\omega} - \nabla \Pi + R^{-1} \nabla^2 \mathbf{v} \quad \text{in } D \tag{1}$$

$$\frac{\partial T}{\partial t} + \nabla \cdot (\mathbf{v} T) = (R\,Pr)^{-1} \nabla^2 T \quad \text{in } D \tag{2}$$

where D is the computational domain; $\mathbf{v}(\mathbf{x}, t) = u\hat{x} + v\hat{y}$ is the velocity; $\mathbf{x}$ and t are the space and time coordinates, respectively; $\Pi = p + 1/2|v|^2$ is the dynamic pressure; $\boldsymbol{\omega} = \nabla \times \mathbf{v}$ is the vorticity and $\nabla^2 = \partial^2/\partial x^2 + \partial^2/\partial y^2$ is the Laplacian operator. Notice that the second derivative term in the streamwise direction has been retained to account for local streamwise variations in periodic, fully developed flows. The Reynolds number is defined as $R = (3/2)VH/\nu$ where ν is the kinematic viscosity, V is the time-mean cross-channel average velocity and H is the half-height of one channel. The Prandtl number is $Pr = \nu/\alpha$, where α is the thermal diffusivity of the fluid. These equations are non-dimensionalized by scaling the velocities by $3/2V$ and the lengths by H. Consequently, the time is non-dimensionalized by the convective time, i.e. the time necessary for a fluid particle traveling with velocity $3/2V$ to move the distance H.

The velocity boundary conditions are Dirichlet on rigid walls and periodic in the streamwise direction which implies that, at a sufficiently large distance from

the entrance, the instantaneous velocity profile starts repeating itself with a periodic length equal to nL. Consequently, the boundary conditions for the velocity $\mathbf{v}(\mathbf{x}, t)$ are

$$\mathbf{v}(\mathbf{x}, t) = 0 \quad \text{on } \partial D_s \tag{3}$$

$$\mathbf{v}(x+nL, y, t) = \mathbf{v}(x, y, t) \quad \text{on } \partial D_p \tag{4}$$

corresponding to no-slip on the solid walls ∂D_s and periodicity on ∂D_p. L is the periodicity of the geometry (Fig. 1) and n is the integer periodicity index of the computational domain which depends on the physically attainable solution.

For steady-state cases, the integer periodicity index n is 1, whereas, to capture the most unstable excited channel mode in time-dependent situations, an integer periodicity index larger than one may be required. This necessitates either experimental corroboration of the numerical simulations or solving the linearized Orr–Sommerfeld equation [15]. The latter gives the linearized Tollmien–Schlichting frequency which is an estimate of the least stable mode compatible with the geometry, enabling us to determine the required computational domain.

For the pressure we require

$$\Pi(\mathbf{x}, t) = -f(t)x + \tilde{\Pi}(\mathbf{x}, t) \tag{5}$$

$$\tilde{\Pi}(x+nL, y, t) = \tilde{\Pi}(x, y, t) \tag{6}$$

where the driving pressure gradient $f(t)$ is determined by imposing the flow rate condition $Q = \int u(x = 0, y, t)\, dy = 8/3$.

The thermal boundary conditions are uniform heat flux at the interrupted plates and adiabatic at the flat walls. For periodic thermally developed domains, the temperature can be decomposed into a linear part and a periodic contribution

$$T(\mathbf{x}, t) = \theta(\mathbf{x}, t) + \gamma x \tag{7}$$

$$\theta(x+nL, y, t) = \theta(x, y, t) \tag{8}$$

where $\gamma = q'/R\,Pr\,Q\,L$, and q' is the total heat transfer rate into the domain. To obtain the appropriate periodic condition for θ, a linear term is subtracted to compensate for the rise in mean temperature based on the mass flow rate due to the net heat flux input.

The numerical approach followed here is that of direct numerical simulation, where the instantaneous unaveraged Navier–Stokes equations are solved and all scales of time variations are resolved. The steady states and supercritical states with self-sustained oscillatory flows are computed using initial value solvers.

The discretization in time is done by a finite-difference, semi-implicit algorithm using a three-step splitting scheme [16]. The convective non-linear term is marched explicitly in time using a third-order Adams–Bashforth scheme, and the pressure and diffusion contributions are treated implicitly by a Crank–Nicolson scheme.

The spatial discretization proceeds using a high-order spectral element method [17], where the computational domain is divided into general quadrangular elements, and the geometry and variables in each element are represented as a tensor product of high-order Lagrangian interpolants through Chebyshev collocation points. The method combines the advantages of both globally unstructured and locally structured spatial discretizations, where the global decomposition in macro-elements allows geometric flexibility and the local structure permits an efficient high-order approximation by spectral techniques with rapid convergence and high accuracy. To generate the system of discrete equations, the convective term is treated by collocation operators, while the elliptic contributions for the pressure and viscosity terms are handled with variational projection operators. More details of this formulation are presented in ref. [6]. Computational efficiency is obtained by using collocation for the non-linear convective term and parallel static condensation for the variationally formulated problem. Static condensation decouples the unknowns at the boundary nodes from those at the interior nodes of the elements, making this procedure very appropriate for implementation in vectorial and parallel computers. A typical computational domain and its spectral element mesh corresponding to $n = 2$ is shown in Fig. 5.

The numerical solutions were obtained using 102 spectral elements with 7×7 Chebyshev collocation points in x and y directions in each element. A typical run of 10 000 time steps of size equal to 8.4×10^{-3}

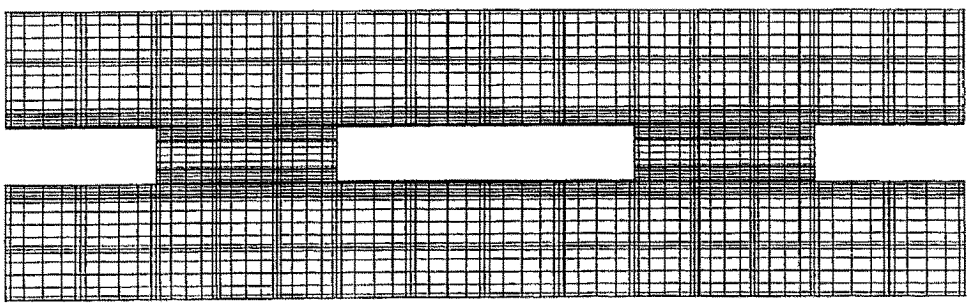

FIG. 5. Computational domain and typical spectral element mesh for the periodic, fully developed communicating-channels numerical simulations.

units of non-dimensional time takes about 6200 CPU seconds on a Cray Y-MP. To account for three-dimensional velocity variations in complex geometries with one homogeneous flow direction, we employ a mixed spectral element–Fourier method [18] where the discretization proceeds by breaking up the computational domain into three-dimensional sub-domains with planar spectral elements in the x–y plane and Fourier expansions in the z direction.

5. RESULTS

Experimental and numerical results describing the flow pattern and temperature field in communicating channels for different flow conditions, specified by the Reynolds number, are presented in this section.

Experimental runs were performed for Reynolds numbers from $R = 120$ to $R = 630$. The electric power supplied to the heaters was varied from 4 to 12 W per foil heater. It was increased with increasing air flow velocities, in order to maintain enough interference fringes necessary for the quantitative evaluation of the interferograms. The high-speed images were recorded on the ninth plate (the leading edge of the tenth plate can also be seen in the pictures) where flow conditions are periodically fully developed.

Numerical simulations correspond to the range of Reynolds numbers from $R = 100$ to $R = 400$. The numerically predicted velocity fields for different flow conditions are shown in Fig. 6, where the flow is from right to left. The steady-state velocity field is shown in Fig. 6(a) for a Reynolds number $R = 150$. It is seen that two counter-rotating vortices are aligned and confined in the communicating (inter-plate) region. Figure 6(b) displays the instantaneous flow field for $R = 175$, where the lower vortex has moved downstream. For the above flow conditions, the flow in the channels is virtually parallel to the flat walls, and there is almost no material exchange between the communicating region and the channel flows. The instantaneous velocity vectors of the non-linear, steady periodic flow at $R = 300$ are plotted in Fig. 6(c). The

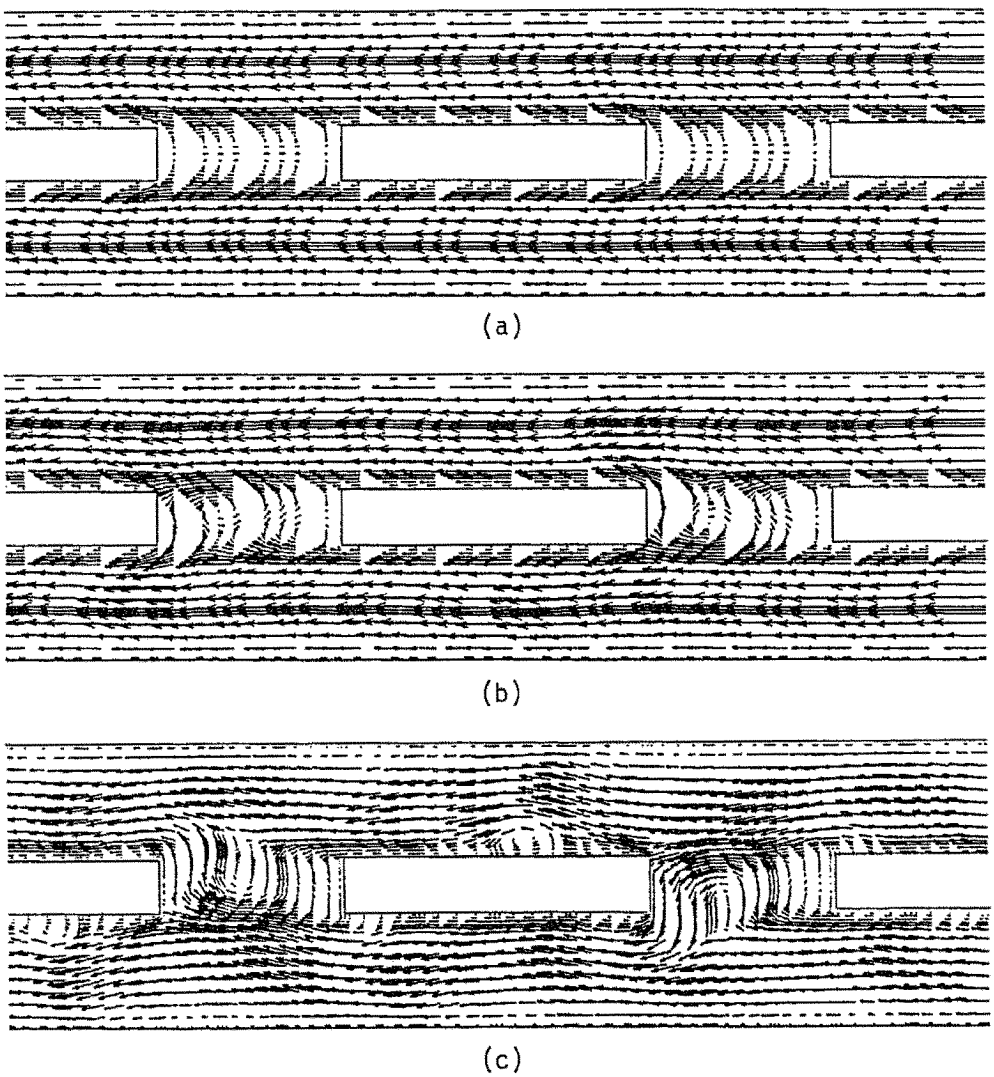

FIG. 6. Instantaneous velocity vectors for (a) $R = 150$, (b) $R = 175$ and (c) $R = 300$, for a $n = 2$ calculation (i.e. periodicity over an interval of $2L$).

wavy character of the flow indicates that the flow has undergone a bifurcation from the steady state of Fig. 6(a) to a time-periodic, self-sustained oscillatory flow. A different vortex dynamics is also seen in the region communicating with both channels, where the vortices are now ejected alternately to the top and bottom channels inducing mixing between the inter-plate and bulk flows.

The behavior of the streamwise velocity as a function of time at $R = 150$, indicates a constantly decaying amplitude (Fig. 7(a)), while at a higher Reynolds number, i.e. $R = 200$, the velocities have converged asymptotically to a periodic state with fixed oscillatory amplitude as shown in Fig. 7(b). This implies that the critical Reynolds number (R_c) for the onset of self-sustained oscillatory flow is between 150 and 200. The decay frequency (Fig. 7(a)) as well as the self-sustained oscillation frequency (Fig. 7(b)) coincides with the least stable Tollmien–Schlichting frequency at the corresponding Reynolds number.

The existence of a geometric spatial periodicity of the flow as well as an oscillatory temporal periodicity should be noted here. For instance, the flow field in Fig. 6(c) indicates three traveling waves per two geometric periodicities (i.e. wavelength $L^* = 2L/3$), whereas the flow in a Lagrangian framework is also periodic in time with a non-dimensional period T given by a typical crest-to-crest or trough-to-trough distance in Fig. 7.

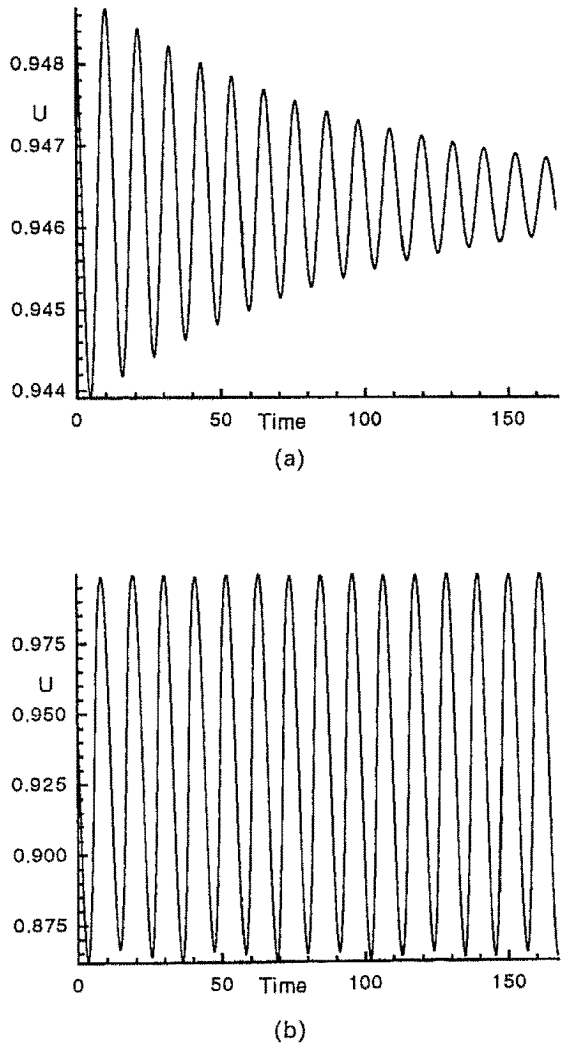

FIG. 7. History of the streamwise u-velocity as a function of time for (a) $R = 150$ and (b) $R = 200$ at $(x/H, y/H) = (4.0, 0.125)$.

The flow velocity in the experiments was varied stepwise. At $R = 145$, no oscillations are observable, whereas, at $R = 200$, mild oscillations appear which corroborate the numerical prediction of the critical Reynolds number range for the onset of self-sustained oscillatory flow.

Figure 8 shows a typical experimental visualization of the instantaneous temperature field. We can recognize different regions relevant to the thermal analysis which also carry information on the oscillatory nature of the flow. In the top (i) and bottom (ii) channels the isotherms are basically parallel to the main channel, with short thermal waves superimposed on long waves traveling in the flow direction. Points A and B represent locations of a traveling maximum and minimum, respectively. The asymmetry in the isotherm waviness in the main channel regions can be attributed to buoyancy effects which are destabilizing in the top channel and stabilizing in the bottom channel. The redevelopment of the thermal boundary layer (iii) is clearly depicted in Fig. 8. In the vortex region (iv), oscillations of the isotherms as well as vortex development at the trailing edge of the plate can be observed. By measuring the frequencies of oscillation of the isotherms, it is possible to determine vortex frequencies as the time between the successive illuminations is known.

A temporal sequence of interferograms recorded at $R = 593$ by high-speed cinematography at a velocity of 600 picture frames per second is shown in Fig. 9. At this Reynolds number, the oscillatory behavior and its influence on the temperature fields can be clearly observed. From the sequence of interferograms, the velocity of wave propagation and the wavelength can be determined by measuring the locations of wave minima and maxima. The oscillatory effects in the top and bottom channels influence the thickness of the thermal boundary layer along the plate and cause its successive compression and expansion. This effect is observable at the leading edge of the plate due to intensive vortex movements in this region. The two counter-rotating vortices between the plates are now in an unstable configuration and are alternately ejected from the inter-plate zone, improving communication between the channels as well as mixing between the vortex region and channel flows. The oscillatory effects discussed for this state are also observed for $R = 366$ and $R = 493$ but with small amplitudes and less pronounced waviness of the isotherms.

In Fig. 10, the amplitude of isotherm extrema vs time for the upper and lower vortex regions is

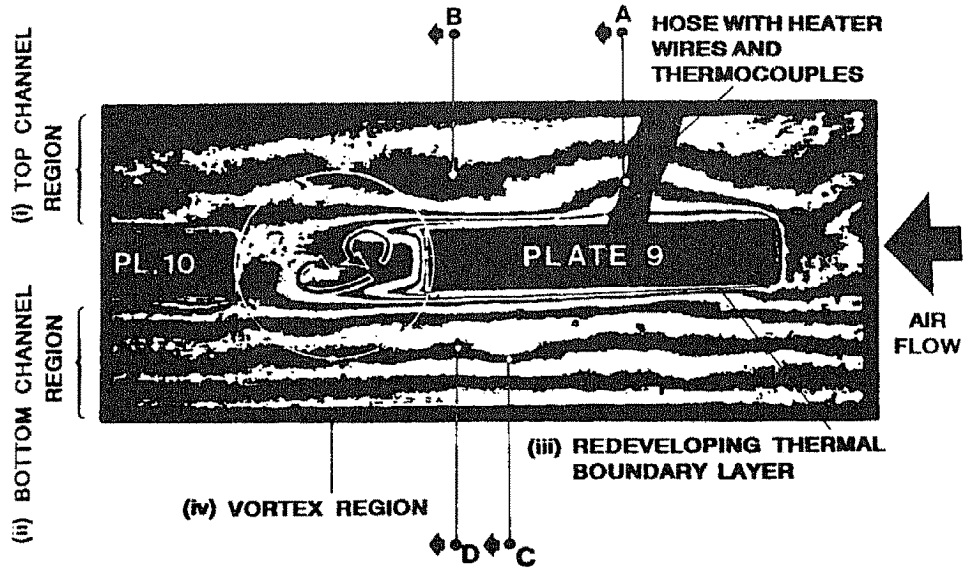

FIG. 8. Interferogram showing a typical experimental visualization of the instantaneous temperature field and its characteristic regions.

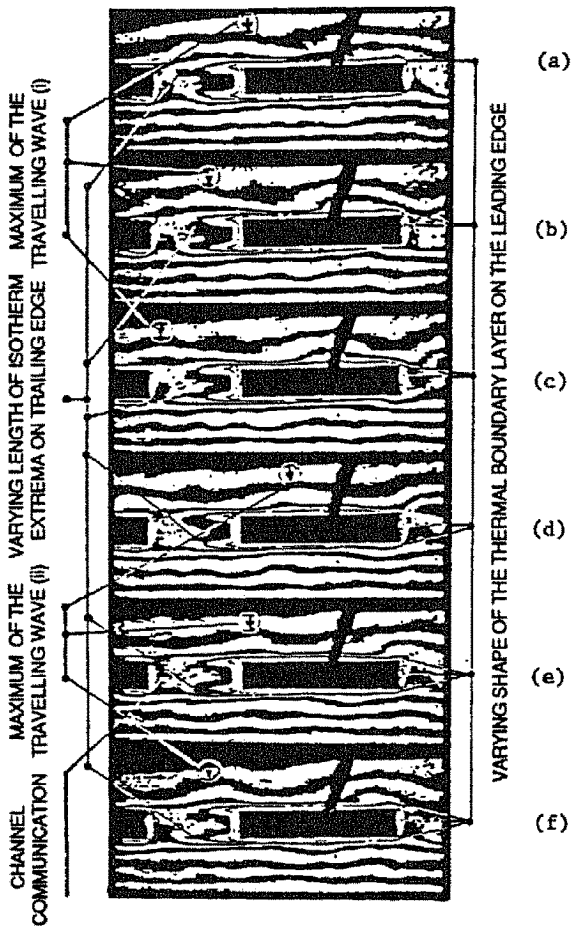

FIG. 9. Temporal sequence of interferograms (a) $t^* = 0$, (b) $t^* = 0.005$ s, (c) $t^* = 0.01$ s, (d) $t^* = 0.015$ s, (e) $t^* = 0.02$ s and (f) $t^* = 0.025$ s; recording velocity 600 frames per second, $R = 593$, $T_p = 79.5$°C. Images obtained with infinite fringe field alignment. Arrows indicate the position of two maxima propagating along the top channel.

presented. These amplitudes were obtained by measuring the locations of isotherm extreme for several periods of oscillations. The oscillatory character can be clearly recognized with the maximum for the upper vortex and the minimum for the lower vortex and vice versa.

The time- and space-averaged Nusselt number, Nu, calculated numerically, is plotted as a function of Reynolds number, R, in Fig. 11. For a fully developed laminar flow in plane channel ($R \lesssim 1200$), the Nusselt number is 1.35, independent of the Reynolds number. Figure 11 indicates that, even for a steady flow of $R = 100$, there is an increase in Nu over the corresponding plane-channel value. Figure 11 also shows that the rate of increase of Nu increases as R is beyond its critical value. This can be explained by considering the fact that in the lower range of R, the flow field is steady. Any increase in Nu over the fully developed, plane-channel value can, therefore, be solely attributed to thin boundary layers. As one goes above the critical Reynolds number, the flow becomes unsteady and oscillatory. This oscillatory flow, together with the successive resumption of the boundary layers, leads to a higher heat transfer augmentation rate with a further increase in the Nusselt number.

The improved heat transfer due to periodic interruptions of the heat transfer surfaces as well as the self-sustained oscillatory flow is followed by an increase in pressure drop compared to those in a plane channel. The increase in pressure drop is caused by higher skin friction due to the periodic restarting of the boundary layer and the creation of separated flow regions. This is indicated in Fig. 12 which shows a plot of the non-

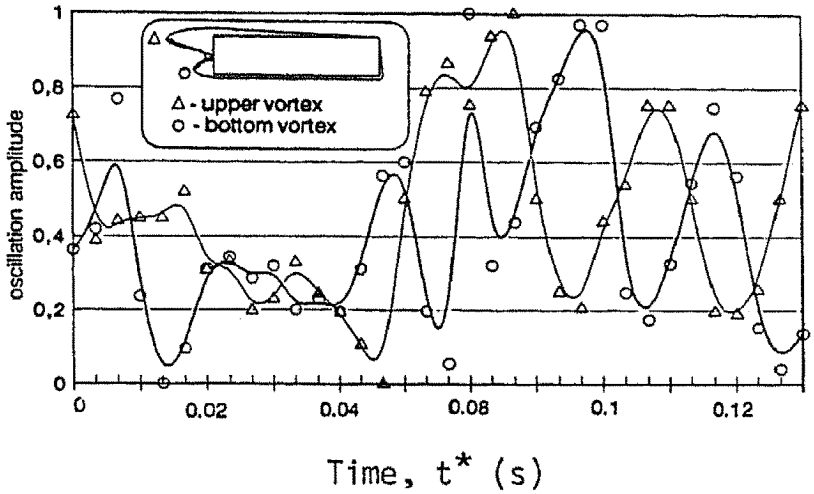

FIG. 10. Amplitudes of isotherm extrema in the vortex region vs time at $R = 593$ (△ upper vortex, ○ bottom vortex).

dimensional measured pressure drop ratio $\Delta p/\Delta p_0$ vs Reynolds number, where Δp_0 is a reference pressure drop corresponding to a fully developed plane channel flow. Initially, the pressure drop *ratio* decreases with the Reynolds number, and it remains nearly constant for Reynolds numbers above 300.

For certain ranges of the Reynolds number, a peculiar flow behavior occurs in this geometry which has not been found before in other self-sustained oscillatory flows [19, 20]. Previously studied self-sustained oscillatory flows typically contain one well-defined frequency that can be determined from history plots such as those shown in Fig. 7 or by their Fourier spectrum. This frequency corresponds to the least stable excited channel mode compatible with the geometry, known as Tollmien–Schlichting (TS) frequency. In the present case, there are two comparable unstable TS modes whose frequencies are manifested in the oscillatory velocity. As shown below by the numerical simulations, these TS modes correspond to wavenumbers $\beta = 2\pi/(L^*/H)$ that comprise either three or four wavelengths per two geometric periodicities $(2L/H)$.

A history plot of the streamwise u-velocity as a function of time at a characteristic point $(x/H = 4.0, y/H = 0.125)$ in the domain for a long simulation at $R = 225$ is shown in Fig. 13 along with the Fourier power spectra at four time intervals (a–d). This plot indicates that the flow asymptotically reaches a stable state. This time signal represents a quasi-periodic state composed of the sum of two periodic functions as indicated by the two peaks located at the fundamental frequencies in the power spectrum plots. These frequencies are non-dimensionalized by the convective time and are related to the corresponding dimensional frequency by

$$\omega_d = (\nu R/H^2)\omega \tag{9}$$

where ω_d and ω are the dimensional and non-dimensional frequencies, respectively. For the present experimental setup, the channel half-height H is 0.005 m (Fig. 1) and the air kinematic viscosity, ν, is taken to be 20.91×10^{-6} m^2 s^{-1} at an average experimental temperature of 80°C. Looking at Fig. 13, one can see that there is a dominant Fourier non-dimensional frequency, $\omega_1 = 0.5753$ (17.23 Hz) which closely matches the TS frequency, $\omega_{TS} = 0.539$ (16.14 Hz), corresponding to $\beta = 1.178$, i.e. three waves per two geometric periodicity lengths.

Next, we show the evolution of the flow structure and temperature fields in a sequence of the time frames (a–c) within the quasi-periodic cycle plotted in Fig. 14.

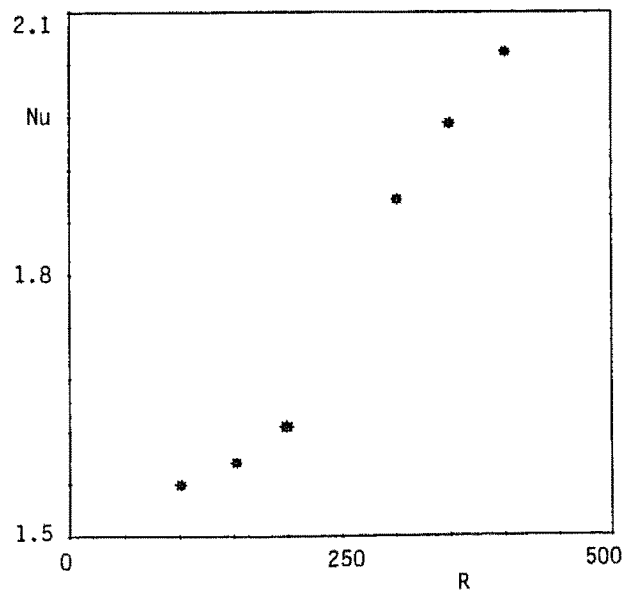

FIG. 11. Time- and space-averaged Nusselt number vs Reynolds number.

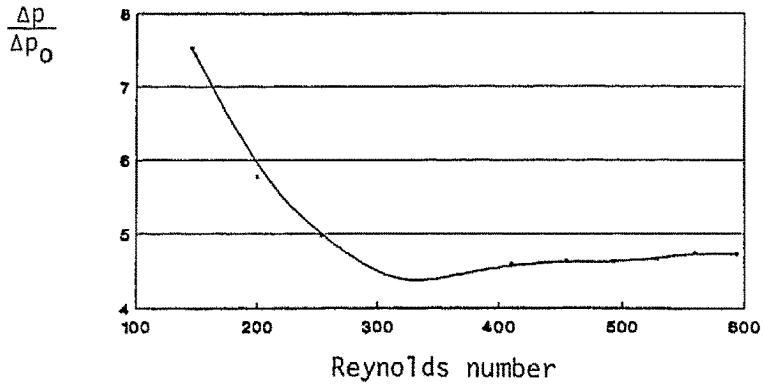

FIG. 12. Pressure drop on the test section scaled by the pressure drop on the basic plane channel geometry vs Reynolds number.

Figure 15 depicts u-velocity profiles across the transverse direction in the upper channel at a particular streamwise location, $x = 1.166$, at various instants of time (a–c) of the quasi-periodic cycle shown in Fig. 14. The velocity profiles have deviated considerably from the plane Poiseuille flow profile, which is also indicated in the figure for comparison. This is due to the effect of the self-sustained oscillations and traveling wave structure.

Figure 16 shows the flow pattern in terms of the instantaneous velocity vectors, and Fig. 17 shows the corresponding instantaneous isotherm plots. These pictures demonstrate the complex separation phenomena, the multiple thermal boundary layer restarting and the effect of the separated flow on the resulting temperature distribution, similar to the behavior of the experimentally obtained isotherm visualizations of Fig. 9. The traveling wave structure as well as the propagation of the thermal wave can be followed up in time through the evolution plots. The vortex dynamics in the communicating regions are synchronized with the wavy flow which, indeed, corresponds to in-phase traveling waves in both channels. The vortices in the communicating regions are ejected alternately to the top and bottom channels removing hot fluid from these regions and, what is more important, enhancing flow mixing. The vortex ejection also affects the flow at the edge of the plate segments, delaying the formation of the thermal boundary layer, and decreasing, therefore, its overall thickness. This can be clearly seen in the temperature fields obtained by numerical simulation in Fig. 17, and is verified by the experimental visualization obtained with interferometry as shown in Fig. 9.

As the Reynolds number is increased further, similar flow patterns are obtained. The mixing is however, stronger, the amplitude of the oscillatory flow increases and the flow at the interrupted plates reverses, separating from the walls as depicted in Fig. 6(c) by the instantaneous velocity field.

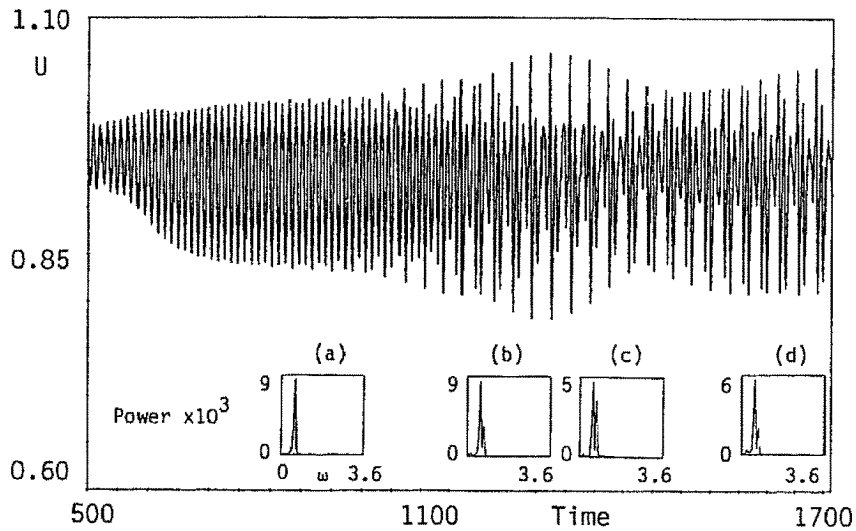

FIG. 13. History of the streamwise u-velocity and its power spectra for $R = 225$ at $(x/H, y/H) = (4.0, 0.125)$.

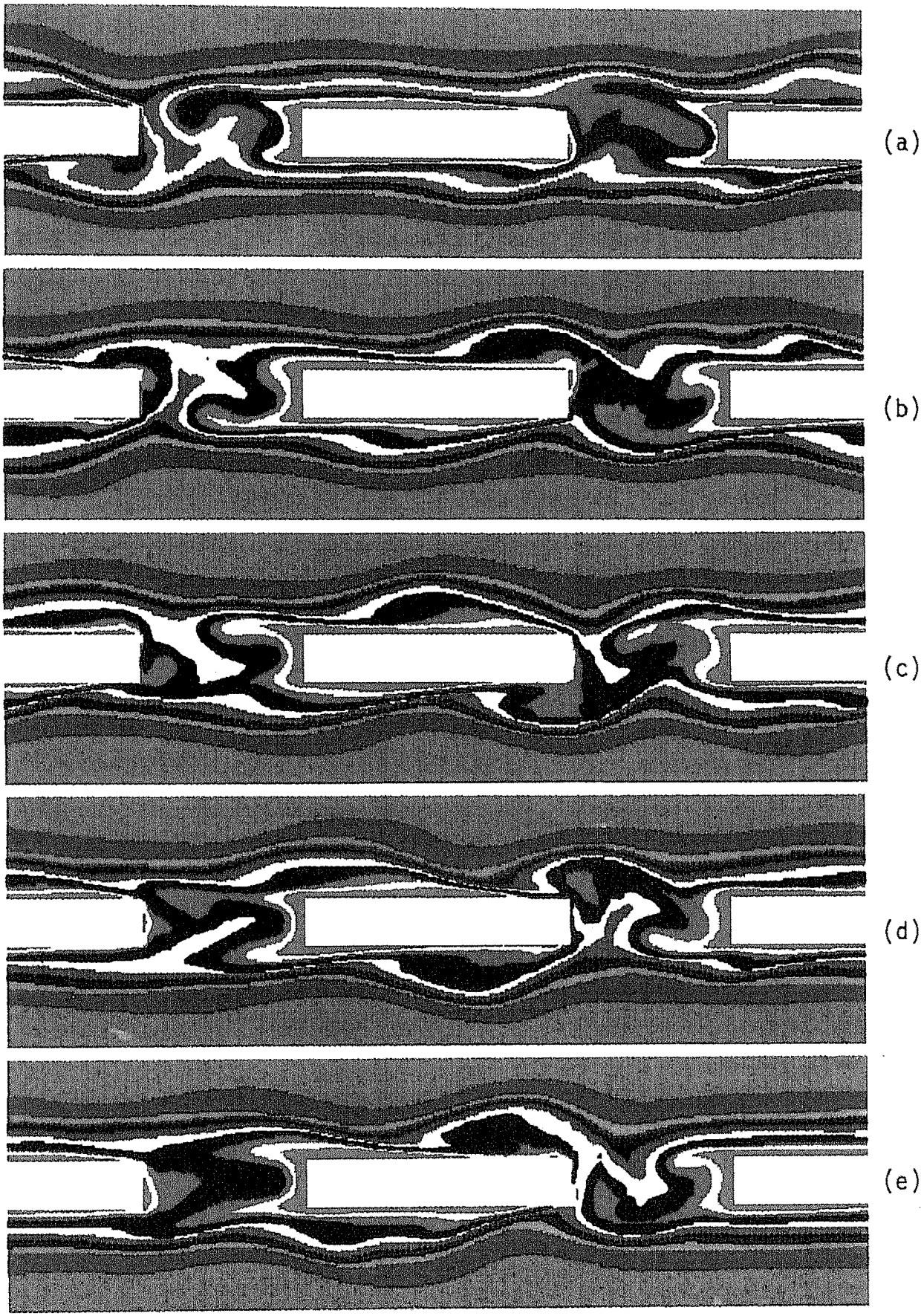

FIG. 17. Instantaneous isotherm plots during the flow quasi-periodic cycle of the self-sustained oscillations corresponding to the flow field of Fig. 16.

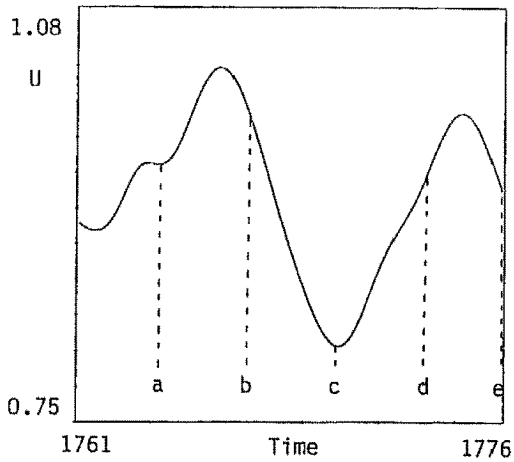

FIG. 14. History of the streamwise u-velocity as a function of time for a quasi-periodic cycle at $(x/H, y/H) = (4.0, 0.125)$.

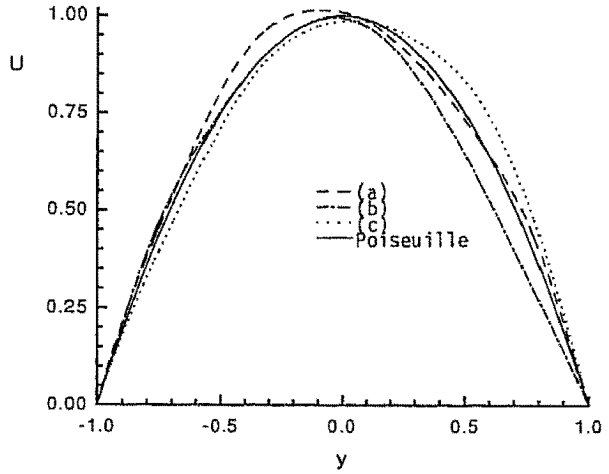

FIG. 15. u-velocity profiles along the transverse direction at a streamwise location $(x/H = 1.1663)$ for various instants of time (a–c) corresponding to the quasi-periodic flow cycle shown in Fig. 14. For comparison, the plane Poiseuille flow profile is also included.

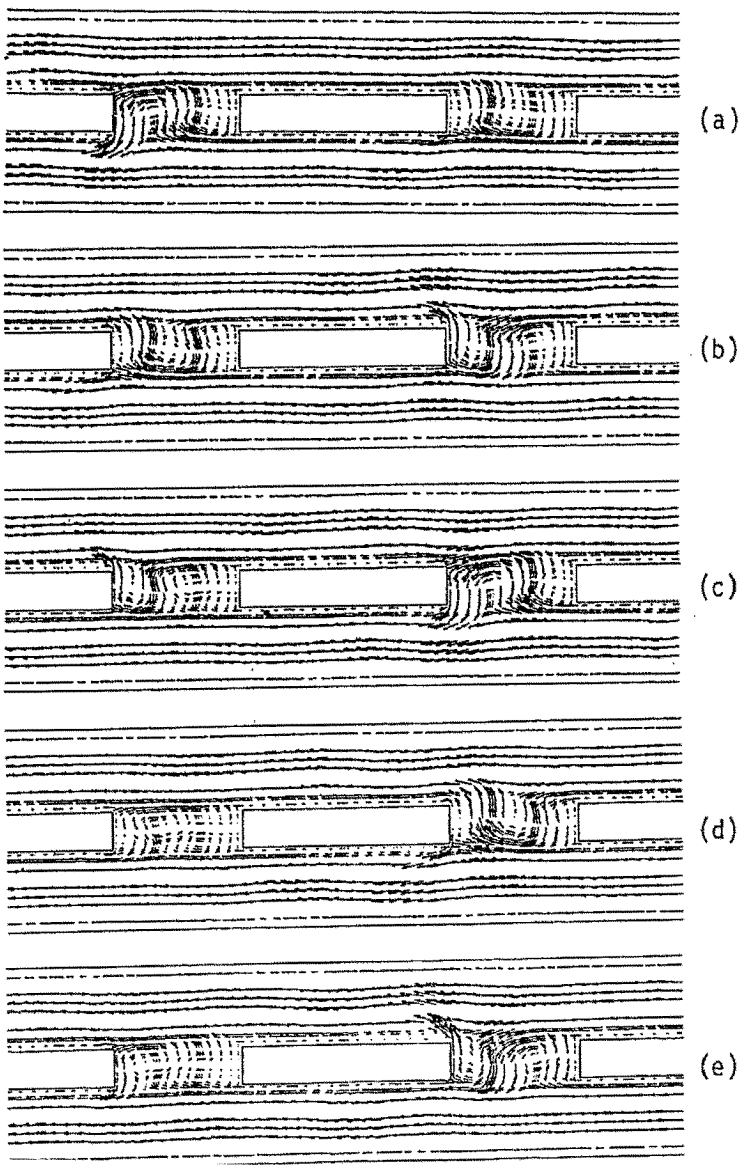

FIG. 16. Instantaneous velocity vectors at $R = 225$ at various times (a–e) during the flow quasi-periodic cycle shown in Fig. 14.

6. CONCLUDING REMARKS

The experimental and numerical results reveal the oscillatory nature and the traveling wave structure of the communicating channels flow when the system is operated above a critical Reynolds number of about 200. Comparisons between the experimental results and the numerical calculations indicate very good agreement about the flow conditions (R_c) for the transition from steady to oscillatory laminar flow and for the onset of self-sustained oscillations in the periodic, fully developed flow region. The frequency of these oscillations and, therefore, the traveling wave speeds, correspond to Tollmien–Schlichting waves compatible with the geometry, excited and sustained by the spatially periodic, geometrically induced flow perturbations. There are two competing, similarly unstable, Tollmien–Schlichting modes excited by the communicating-channels geometry reported in this work.

It has been shown that communicating channels composed of interrupted surfaces offer important heat transfer performance advantages over plane channels. They generate thinner thermal boundary layers as well as enhance mixing due to self-sustained oscillations, ejection of vortices and interaction between communicating channels.

Acknowledgement—This work was supported by the National Science Foundation under Grant No. CTS-8908808, the Engineering Design Research Center at Carnegie Mellon University under cooperative agreement EDC-8943164, and the KFA Jülich and the Yugoslav Science Fund through a bilateral Germany–Yugoslavia project. Some of the computations were performed on the Cray Y-MP under grant CBT 900010P Cray Research Inc. at the Pittsburgh Supercomputer Center.

REFERENCES

1. W. M. Kays and A. L. London, *Compact Heat Exchangers*. McGraw-Hill, New York (1984).
2. E. M. Sparrow, B. R. Baliga and S. V. Patankar, Heat transfer and fluid flow analysis of interrupted wall channels, with application to heat exchangers, *J. Heat Transfer* **99**, 4–11 (1977).
3. D. P. Sekulic, Flow through communicating channels compact heat transfer geometry, *Int. Commun. Heat Mass Transfer* **16**, 607–619 (1989).
4. R. M. Manglik and A. E. Bergles, The thermal-hydraulic design of the rectangular offset-strip-fin compact heat exchanger, *A. L. London Symposium on Compact Heat Exchangers*, Stanford University (1989).
5. C. H. Amon and B. B. Mikic, Numerical prediction of convective heat transfer in self-sustained oscillatory flows, *J. Thermophys. Heat Transfer* **4**, 239–246 (1990).
6. C. H. Amon and B. B. Mikic, Spectral element simulations of unsteady forced convective heat transfer: Application to compact heat exchanger geometries, *Numer. Heat Transfer* **19**, 1–19 (1991).
7. D. Majumdar and C. H. Amon, Heat and momentum transport in oscillatory viscous flows. In *Heat Transfer in Unsteady Flows* (Edited by L. S. Yao and J. O'Brien), Vol. 158, pp. 1–8. ASME HTD (1991). To appear in *J. Heat Transfer*.
8. H. M. Joshi and R. L. Webb, Heat transfer and friction in the offset strip-fin heat exchanger, *Int. J. Heat Mass Transfer* **30**, 69–84 (1987).
9. S. V. Patankar, C. H. Liu and E. M. Sparrow, Fully developed flow and heat transfer in ducts having streamwise-periodic variations of cross-sectional area, *J. Heat Transfer* **99**, 180–186 (1977).
10. C. V. Herman, F. Mayinger and D. P. Sekulic, Experimental verification of oscillatory phenomena in heat transfer in a communicating-channel geometry, *2nd World Conf. on Experimental Heat Transfer, Fluid Mechanics and Thermodynamics*, Dubrovnik, Yugoslavia (1991).
11. W. Hauf and U. Grigull, Optical methods in heat transfer. In *Advances in Heat Transfer*, Vol. 6. Academic, New York (1970).
12. F. Mayinger and W. Panknin, Holography in heat and mass transfer, *Proc. Fifth Int. Heat Transfer Conf.*, Tokyo, Japan, pp. 28–43 (1974).
13. C. M. Vest, *Holography Interferometry*. Wiley, New York (1979).
14. F. Mayinger and Y. M. Chen, Heat transfer at the phase interface of condensing bubbles, *Proc. Eighth Int. Heat Transfer Conf.*, San Francisco, California, pp. 1913–1918 (1986).
15. P. G. Drazin and W. H. Reid, *Hydrodynamic Stability*. Cambridge University Press, Cambridge (1981).
16. S. A. Orszag and L. C. Kells, Transition to turbulence in plane Poiseuille and plane Couette flows, *J. Fluid Mech.* **96**, 159–205 (1980).
17. A. T. Patera, A spectral element method for fluid dynamics: laminar flow in a channel expansion, *J. Comput. Phys.* **54**, 468–477 (1984).
18. C. H. Amon, Spectral element-Fourier method for transitional flow in complex geometries, *Proc. 10th AIAA Computational Fluid Dynamics Conference*, pp. 915–925 (1991). To appear in *AIAA J.*
19. N. K. Ghaddar, K. Z. Korczak, B. B. Mikic and A. T. Patera, Numerical investigation of incompressible flow in grooved channels. Part 1. Stability and self-sustained oscillations, *J. Fluid Mech.* **163**, 99–127 (1986).
20. C. H. Amon and A. T. Patera, Numerical calculation of stable three-dimensional tertiary states in grooved-channel flow, *Physics Fluids A* **1**, 2005–2009 (1989).

ETUDE NUMERIQUE ET EXPERIMENTALE D'ECOULEMENTS AUTO-ENTRETENUS DANS DES VEINES COMMUNICANTES

Résumé—Une étude des écoulements et phénomènes thermiques dans des veines communicantes, combinant une approche numérique et expérimentale, est effectuée dans le but de comprendre le comportement des surfaces d'échange de chaleur compactes avec plaques interrompues. Les paramètres géométriques sont définis afin d'exciter et d'entretenir des modes normalement amortis de Tollmien–Schlichting. A des nombres de Reynolds relativement faibles, une propagation d'ondes générant des écoulement oscillants autoentretenus, qui améliorent sensiblement le mélange, est observée. Le nombre de Reynolds critique à partir chequel des oscillations commencent à être observées pour un écoulement périodique et entièrement développé est déterminé. Les résultats numériques sont obtenues par une simulation directe des équations, dépendantes du temps, d'énergie et de Navier et Stokes à partir d'une méthode de Fourier avec éléments spectraux. Le phénomène de transfert thermique oscillatoire est visualisé expérimentalement par une interférométrie holographique en temps réel. Les champs thermiques, rélatifs à un écoulement périodique et entiérement développé, ont été filmés à l'aide d'une caméra ultra-rapide. Les visualisations expérimentales des ondes thermiques vérifient les prédictions numériques de la structure thermohydraulique et l'évolution des écoulements dans les veines communicantes.

KOMBINIERTE NUMERISCHE UND EXPERIMENTELLE UNTERSUCHUNG VON SELBSTERREGTEN SCHWINGUNGEN IN DER STRÖMUNG IN KOMMUNIZIERENDEN KANÄLEN

Zusammenfassung—Es wurde eine kombinierte numerische und experimentelle Untersuchung von Strömungsfeldern und Wärmetransportvorgängen in kommunizierenden Kanälen durchgeführt, um Einsicht in das Verhalten der kompakten wärmeaustauschenden Flächen mit geschlitzten Platten zu gewinnen. Die geometrischen Parameter wurden so gewählt um die sonst gedämpften Tollmien–Schlichting Schwingungen anzuregen und aufrecht zu erhalten. Es wurden schon bei relativ niedrigen Reynolds-Zahlen Wanderwellen beobachtet, die die selbsterregten Schwingungen verursachen und dadurch die Durchmischung des Fluids wesentlich verbessern. Die kritische Reynolds Zahl im Bereich der periodisch voll entwickelten Strömung, bei welcher die Schwingungen auftreten, wurde bestimmt. Die numerischen Ergebnisse wurden mit Hilfe der direkten numerischen Simulation der zeitabhängigen Energie- und Navier–Stokes Gleichungen erhalten, und dafür wurde die Spektralelementen–Fourier Methode eingesetzt. Die Sichtbarmachung der Schwingungen in dem Wärmeübergangsprozeß erfolgte experimentell, mit Hilfe der echtzeit-holographischen Interferometrie. Die Temperaturfelder in periodisch voll entwickelten Strömungsbedingungen wurden mit einer Hochgeschwindingkeitskamera aufgenommen. Die experimentelle Sichtbarmachung der thermischen Schwingungen bestätigt die numerischen Prognosen der thermischen Striktur dieser Strömung sowie das Verhalten der Strömung in den kommunizierenden Kanälen.

ЧИСЛЕННОЕ И ЭКСПЕРИМЕНТАЛЬНОЕ ИССЛЕДОВАНИЕ САМОПОДДЕРЖИВАЮЩИХСЯ КОЛЕБАТЕЛЬНЫХ ТЕЧЕНИЙ В СООБЩАЮЩИХСЯ КАНАЛАХ

Аннотация—Численно и экспериментально исследуются поля течения и тепловые явления в сообщающихся каналах с целью анализа работы поверхностей компактных пластинчатых теплообменников. Выбраны геометрические параметры, при которых возбуждаются и поддерживаются затухающие моды Толлмиена–Шлихтинга. В результате бегущие волны наблюдаются при сравнительно низких числах Рейнольдса, что приводит к возникновению самоподдерживающихся колебательных течений, которые существенно интенсифицируют смешивание. Определяется критическое число Рейнольдса, при котором начинаются колебания в области периодического полностью развитого течения. Численные результаты получены посредством прямого численного моделирования нестационарных уравнений энергии и Навье–Стокса методом Фурье–анализа. Визуализация теплопереноса при колебательном движении осуществляется с помощью голографической интерферометрии в реальном масштабе времени. В условиях периодического полностью развитого течения температурные поля регистрируюяся с использованием высокоскоростной киносъемки. Данные по визуализации тепловых волн подтверждают результаты численного определения структуры и зволюции течений в сообщающихся каналах.